Construction and Building Materials 490 (2025) 142143

Contents lists available at ScienceDirect

Construction and Building Materials

journal homepage: www.elsevier.com/locate/conbuildmat

# Sensitivity of bending stiffness to moisture content in adhesive-free wooden-doweled cross-laminated timber panels

Angelo Aloisio [a,*], Dag Pasquale Pasca [b], Roberto Tomasi [c], Massimo Fragiacomo [a]

[a] Department of Civil, Construction-Architectural and Environmental Engineering, Università degli Studi dell'Aquila, L'Aquila, Italy
[b] Norsk Treteknisk Institutt (Norwegian Institute of Wood Technology), Oslo, Norway
[c] Faculty of Science and Technology, Norwegian University of Life Sciences, Norway

ARTICLE INFO

*Keywords:*
Wooden dowels
Cross-laminated timber
Adhesive-free
Moisture
Sustainability

ABSTRACT

Despite the rapid commercial success of cross-laminated timber (CLT) in the past decade, largely thanks to its excellent thermal and structural performance, the use of synthetic adhesives still raises sustainability concerns, in particular with respect to fire behavior of the bond lines, potential VOC emissions during service, and the challenges of separating bonded layers at end-of-life for recycling or energy recovery. While wooden-doweled CLT has never been considered a viable large-scale alternative to traditional CLT, it is important to better understand the properties of adhesive-free CLT panels as potential surrogates. In the case of wooden-doweled CLT, the mechanical integrity of the panel depends on the assembly conditions, where the moisture content of the dowels at insertion is lower than that of the timber boards. The swelling of the dowels, as they equilibrate with the moisture content of the surrounding timber, ensures the structural performance of the panel. However, what happens if there is a general decrease in moisture content over the building's lifespan and the differential shrinkage between the boards and dowels compromises the structural integrity? In this study, the authors tested adhesive-free wooden-doweled CLT panels, assessing the sensitivity of the bending stiffness to three moisture content scenarios: 8, 12 and 15%. Using classical methods for predicting the stiffness of layered beams, such as the $\gamma$ and the shear analogy methods, the authors indirectly estimated the slip modulus based on three-point bending tests and modal parameters as a function of wood moisture content. Thus, the paper, examining the mechanical behavior of wooden-doweled CLT panels under varying moisture content conditions, provides practical recommendations for their use.

## 1. Introduction

Cross-laminated timber (CLT) has gained widespread attention as a high-performance engineered wood product with promising applications in structural systems [1,2]. CLT construction has been shown to result in lower greenhouse gas emissions compared to conventional systems, as demonstrated by life-cycle analysis (LCA) studies [3]. The panels are effectively used in buildings located in seismic regions, serving both as walls and floors [4,5].

State-of-the-art CLT manufacturing typically involves the use of synthetic adhesives such as phenol-formaldehyde (PF) or polyurethane (PUR) [6], which provide high structural performance but present challenges under fire conditions [7], during end-of-life recycling [8], and in terms of emissions of volatile organic compounds (VOCs) and formaldehyde [9]. Despite representing only a small fraction of the panel's mass, adhesives contribute substantially to the overall environmental impact of CLT [8,9]. Alternatives such as lignin-based binders show promise but require blending with phenol for comparable performance [10], and solvent-based formulations must be handled with caution [11].

As a result, there is growing interest in adhesive-free CLT systems, particularly those relying on mechanical connectors such as wooden dowels, which offer a different set of structural and design challenges. This study investigates the mechanical performance of dowel-laminated CLT panels under varying Moisture Content levels.

## 2. Literature background and research question

Adhesive-free CLT panels offer enhanced recyclability, improved reusability, and reduced environmental impact. Metal fasteners like screws or metal dowels are commonly used for their high load-bearing capacity and structural stability. While metal connectors have proven

* Corresponding author.
*E-mail addresses:* angelo.aloisio1@univaq.it (A. Aloisio), dpa@treteknisk.no (D.P. Pasca), dkr@treteknisk.no (R. Tomasi), massimo.fragiacomo@univaq.it (M. Fragiacomo).

https://doi.org/10.1016/j.conbuildmat.2025.142143
Received 7 March 2025; Received in revised form 3 June 2025; Accepted 4 June 2025
Available online 10 July 2025

performance and wide adoption, the industry is exploring wood-based connectors, such as dowels, timber pegs and nails, as an eco-friendly alternative [12,13]. Wood-based connectors demonstrate full compatibility with the wood material, facilitating disassembly and improving recyclability. Research is ongoing to evaluate the feasibility and performance of wood-based connectors in CLT construction. Versions of CLT using hardwood dowels, such as dowel-laminated timber (DLT) or doweled cross-laminated timber (DCLT), have already been introduced in the market and used in construction.

However, opportunities for innovation, like using CLT assembled with hardwood nails, are yet to be fully explored. Preliminary studies have demonstrated the efficiency of doweled cross-laminated panels (DCLP) for structural use [14]. However, design codes for DCLP are not yet available in current European standards [8]. Investigating the earthquake behavior of buildings made from dowel-laminated timber (DLT) elements, researchers have highlighted that the remaining load-carrying capacity of DLT compared to solid wood may be only 25% depending on the fastener diameter [15]. Salvaged plywood tenons have also been effectively used as connectors in DLT, resulting in a 40% increase in bending stiffness compared to unconnected members [16].

Parametric studies on numerical models have examined the influence of dowel diameter and spacing on the stiffness and maximum load capacity of dowel-laminated timber members [17]. Experimental investigations have confirmed that compressed wood dowels with larger diameters and a higher number of dowels lead to an increase in the flexural modulus of adhesive-free laminated timber (AFLT) beams and adhesive-free cross-laminated timber (AFCLT) panels [18]. However, dowel insertion angles and dowel species do not seem to affect the structural properties [18] substantially. Research on optimizing dowel patterns, shapes, and numbers is yet to be conducted. Normally, the dowel is hydraulically hammered into pre-drilled holes with slightly smaller diameters. Still, recently, dowel welding by high-speed rotation has been explored as a method to join wood dowels with layers. The friction triggered by the rotation of the dowel generates heat at the contact interfaces, leading to lignin softening in the contact region and forming a weld-line after the material cools down [9]. The welding process gives the fastener a non-negligible withdrawal strength, allowing for simultaneous exploitation of both axial and transversal resisting mechanisms of the fasteners, leading to better mechanical performance [19,20]. Still, the durability of welded joints is doubtful, and resins are often combined with welding to obtain acceptable performances [21]. It has been demonstrated that two-layer doweled beams with welded timber dowels can outperform nailed beams of the same length, even when twice as many nails are used as dowels. An original manufacturing process, where dowels are submerged in sunflower oil before being used as part of a rotational welding technique, has shown efficiency in composite action, measured using stiffness relative to a fully composite system, between 49% and 74% [22].

Most studies show that the failure of the composite elements is due to dowel fracture, and hardwood fasteners in softwood layers may further increase performance. Some studies highlighted how the connection performance may be reduced by the dowel shrinkage caused by decreasing ambient humidity [8]. This effect can be avoided using densified wood dowels prone to swelling. Thus allowing for insertion in holes even larger than the dowel itself and consequently easing the manufacturing process [23]. Currently, most research focuses on manufacturing and mechanical performance, while aspects like long-term reliability under variable environmental conditions, fatigue, and fire resistance are not fully addressed. Despite wood-based connectors not being widely adopted in the industry, ongoing investigations strive to establish the reliability of adhesive-free CLT. This alternative addresses concerns about adhesive toxicity while acknowledging that metal connector alternatives may pose recycling challenges [8].

Most studies on pre-wood dowel-type connections focus either on the mechanical behavior of the dowel within the connection or on moment-resisting joints. However, research on their application in CLT panels remains limited. Wooden dowels mainly bear four types of loads: bending, embedment, shear, and axial forces (the latter may arise from friction between the dowel and the timber members [24]). Many studies have examined dowel-type timber joints [25–35], focusing on failure modes [36,37], shear capacity under various failure conditions [38], and factors influencing shear capacity [39,40]. Research indicates that shear capacity is affected by the type and diameter of the dowel and the processing methods used.

Despite the growing scientific interest in adhesive-free solutions, their application remains primarily confined to research [41], with few industrial entities dedicated to their production and commercialization. One of the main challenges of adhesive-free wooden-doweled CLT (WDCLT) is its complete reliance on friction to ensure mechanical interlayer bonding. However, friction is strongly influenced by dowel swelling, which, in turn, depends on hygrothermal conditions, affecting both dimensional stability and structural performance.

To the best of the authors' knowledge, no systematic experimental study has investigated the sensitivity of adhesive-free WDCLT panels to moisture content (MC) variations. Therefore, the main objectives and novel contributions of this study are:

1. Evaluate the sensitivity of WDCLT bending stiffness to MC variations, considering three scenarios (8%, 12%, and 15% MC).
2. Analyze the influence of loading type by estimating bending stiffness through both dynamic identification tests and static three-point bending tests.
3. Assess the accuracy of the $\gamma$-method and the shear analogy method in predicting bending stiffness, using slip modulus values obtained from push-out tests.
4. Compare the bending stiffness of WDCLT with traditional glued CLT panels having an analogous layup.

## 3. Wooden doweled cross-laminated timber panels

The wooden dowel CLT (WDCLT) adhesive-free panel, produced by Biohabitat srl [42], is a solid mass timber panel composed of layers of *Picea abies* boards, each 150 mm wide and 30 mm thick. These layers are arranged in vertical, horizontal, and diagonal orientations. They are mechanically bonded by pressing beech dowels, 16 mm in diameter, into place. The jack applies a hydraulic pressure of 3.04 MPa (30 atm) to insert the dowel into the timber layers. It should be noted that the 30 atm value refers to the internal pressure within the hydraulic system, not to the mechanical stress on the dowel.

The production process for these panels follows a sequence similar to that used by manufacturers like Thoma GmbH in Austria. It begins with the fabrication of the dowels. The 16 mm dowels are shaped using a lathe, cut to the required length, and oven-dried for at least 48 h. The oven-drying process refers to conditioning the specimens at $103 \pm 2\,^{\circ}\mathrm{C}$, following standard procedures for moisture content determination [43,44].

This drying process reduces their MC and causes a slight shrinkage in diameter. The boards are air-dried naturally for 8 months and then kiln-dried until their internal MC is no higher than 10%. Once the dowels are ready, the panel layers are assembled. The edges of the panels are compressed using hydraulic jacks to tightly press the lamellae together, minimizing any gaps between them. A uniform load is applied to the top surface to prevent the boards from lifting during assembly. Holes are pre-drilled with a 10 mm bit, followed by final drilling. After inserting the beech dowels under pressure of up to 30 atm, they are sprayed with water to swell and ensure a tight fit. They are then stabilized along with the boards at a moisture level of around 12%. Finally, the completed panels are left to air dry for about a month, allowing the MC of the lamellae and dowels to equalize (see Fig. 1).

The wall can be produced in various thicknesses, ranging from 150 mm to 270 mm, as shown in Fig. 2. The most commonly used thicknesses are 180 mm and 210 mm, with 150 mm typically used

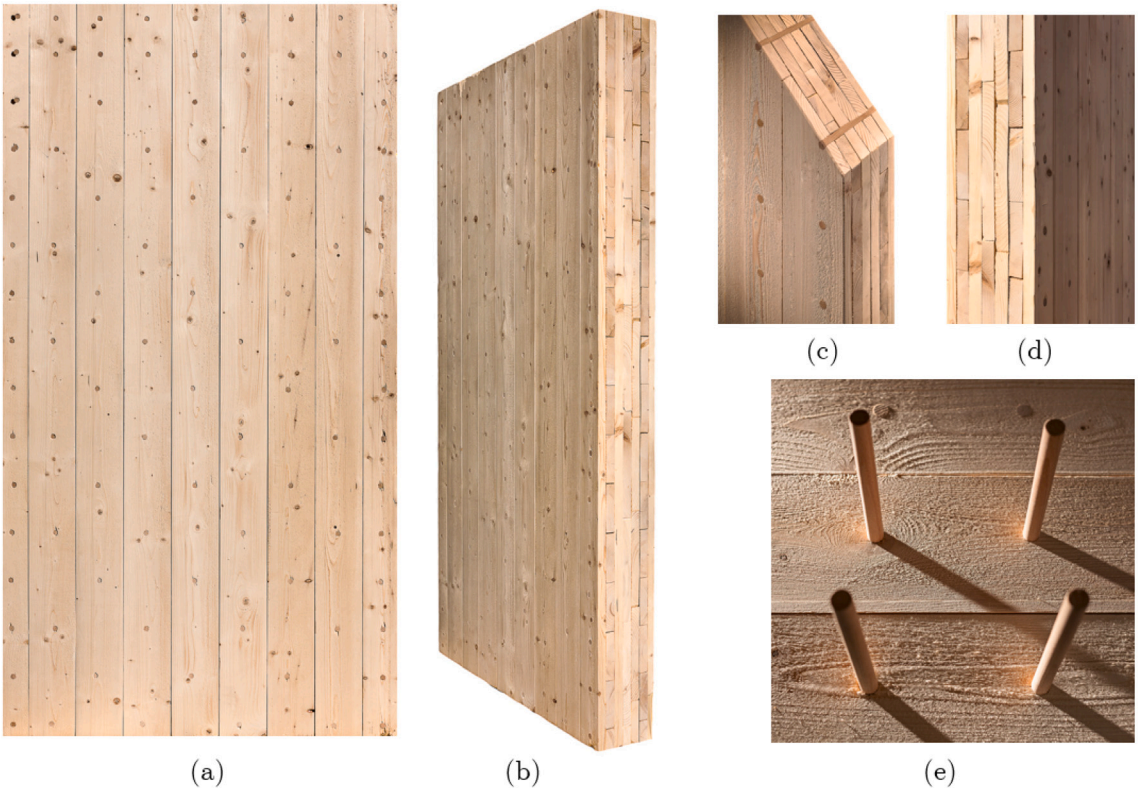


**Fig. 1.** Views of the wooden dowel CLT panels and details of the structural element. (a) front view, (b) lateral view, (c) cross-section with dowel, (d) cross-section without dowel, (e) Dowel in position before insertion.

for internal load-bearing walls. The panels' layup is shown in Fig. 2, with the outer layers always oriented vertically. The beech dowels connecting the layers are positioned around the perimeter of the wall at each board intersection (with a spacing of 150 mm) and alternately in the central part at every second intersection (with a spacing of 300 mm).

In this study, panels with 150 mm and 210 mm thicknesses were used, each measuring 0.5 m wide and 2 m high, with four samples for each panel size.

## 4. Methodology

### 4.1. Problem formulation

This study aims to estimate the sensitivity of the bending stiffness of adhesive-free WDCLT panels to variations in the wood MC. Hereafter, these panels will be referred to as WDCLT for brevity. As explained in the previous section, the mechanical integrity of WDCLT panels is closely linked to the MC of the dowels. The wooden dowels are oven-dried before being used to assemble the boards. Their swelling, caused by reabsorbing moisture from the environment, ensures the mechanical tightness of the assembly. However, what happens if the MC of both the boards and the wooden dowels decreases? Beech wood and Norwegian spruce have different moisture absorption coefficients, meaning that changes in overall MC can alter the panel's mechanical stability. Furthermore, heating systems are often active for much of the year in wooden buildings, especially in colder regions like North America and Central Europe. These systems can significantly reduce the MC so that the MC can drop below 7% in internal panels, while external ones generally range from 7% to 9% [45].

Thus, understanding the effect of MC is crucial, as it can compromise the panel's mechanical and thermal performance. To isolate this phenomenon, the authors conducted controlled experiments rather than reproducing the typical conditions of a building, where daily and seasonal fluctuations in temperature and humidity occur, along with additional layers in the building envelope. For this purpose, a climate chamber was used to condition the panels to specific MC levels. Bending stiffness was then measured before and after the moisture variation. The bending stiffness was measured using the classic three-point bending test and, indirectly, by measuring the frequency of the first three vibration modes. This approach allowed the authors to estimate stiffness under various levels of deformation, whether due to environmental factors or human-induced excitations (e.g., walking or running), as well as from bending tests. The procedure followed three main phases: (i) Dynamic identification tests under ambient excitation and walking in a pinned-pinned configuration. (ii) Three-point bending tests, (iii) Panel conditioning in a climate chamber. These tests were repeated for different MC levels. The slip modulus was estimated using the $\gamma$ and Shear Analogy methods (SAM) by inverting the predictive relationships for bending stiffness, as briefly summarized in the following subsections. The authors estimated the prediction error of the bending stiffness using the slip modulus from push-out tests. Subsequently, an optimization problem was solved to find the optimal multiplier of the slip modulus for each test configuration. This allowed for understanding the effect of excitation level (static vs dynamic) and MC on the slip modulus relative to the reference value obtained from push-out tests.

### 4.2. Literature background on bending stiffness prediction

#### 4.2.1. $\gamma$-Method

The $\gamma$-method, outlined in Appendix B of Eurocode 5, offers a simplified approach for calculating the flexural properties of mechanically connected beams. It is based on the concepts of effective bending stiffness and a connection efficiency factor, and it allows evaluation of the mechanical behavior of beams composed of up to three individual

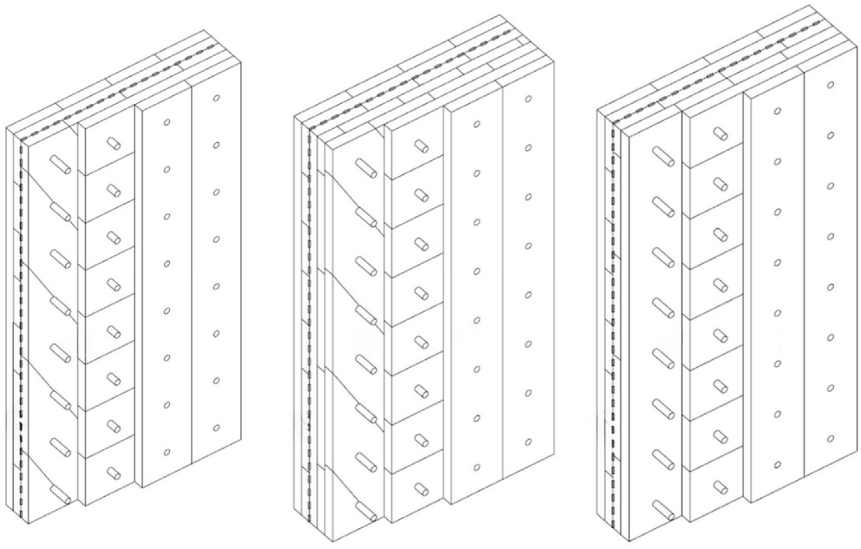

| | | | |
|---|---|---|---|
| Thickness [mm]: | 150 | 180 | 210 |
| No. of Layers: | 5 | 6 | 7 |
| Layup: | (P-O-D1-O-P) | (P-O-P-D1-O-P) | (P-O-P-D1-D2-O-P) |

P=parallel; D1= diagonal 30°; D2=diagonal 150°; O=orthogonal

**Fig. 2.** Layups of the Wooden Dowel CLT panels produced by BIOHABITAT.

members connected by semi-rigid fasteners [46]. This formulation, as discussed by Kreuzinger [47], is most accurate when applied to three-layer beams under simple support conditions, with continuous fasteners of constant stiffness and sufficiently large spans so that shear deformations are negligible. The effective bending stiffness is given by:

$$(EI)_{ef} = \sum_{i=1}^{n} \left( E_i \cdot I_i + \gamma_i \cdot E_i \cdot A_i \cdot a_i^2 \right) \tag{1}$$

Here, $E_i$ is the modulus of elasticity of the $i$th layer, $I_i$ its moment of inertia, $A_i$ its cross-sectional area, $a_i$ the distance from its centroid to the neutral axis of the assembly, and $n$ the total number of layers. In this study, the authors extend the method to include all plies of 5- and 7-layer WDCLT panels, treating each layer explicitly in the model rather than grouping them. The connection efficiency factor $\gamma_i$ is calculated as:

$$\gamma_i = \left( 1 + \frac{\pi^2 \cdot E_i \cdot A_i \cdot s_i}{K_i \cdot l^2} \right)^{-1} \tag{2}$$

where $s_i$ is the spacing between connectors, $K_i$ is the slip modulus of the connection, and $l$ is the span length.

#### 4.2.2. Shear Analogy Method (SAM)

Introduced by Kreuzinger in 1999 [48], the Shear Analogy Method (SAM) offers a more refined approach to calculating the flexural properties of mechanically connected beams. While both SAM and the $\gamma$-method consider factors such as the number of layers and the presence of mechanical fasteners, a key advantage of SAM is its ability to explicitly incorporate the shear deformations of individual layers [47]. This makes it particularly suitable for cases where shear flexibility significantly affects the global response.

In the SAM, the composite beam is modeled as two virtual beams, labeled A and B, coupled through vertical deflections via infinitely rigid web elements. Beam A is assumed to be infinitely stiff in shear, while beam B accounts for the shear flexibility of each layer and the connections.

The bending stiffness of beam A, $B^A = (EI)_A$, includes the inherent bending stiffness of the individual layers:

$$B^A = \sum_{i=1}^{n} \left( E_i \cdot I_i \right) = \sum_{i=1}^{n} \left( E_i \cdot \frac{b_i \cdot h_i^3}{12} \right) \tag{3}$$

$$S^A = \infty \tag{4}$$

The bending stiffness of beam B, $B^B = (EI)_B$, reflects the so-called Steiner terms, based on the distance from the centroid of each layer to the neutral axis:

$$B^B = \sum_{i=1}^{n} \left( E_i \cdot A_i \cdot z_{si}^2 \right) = \sum_{i=1}^{n} \left( E_i \cdot b_i \cdot h_i \cdot z_{si}^2 \right) \tag{5}$$

Note: $z_{si}$ is equivalent to $a_i$ in the $\gamma$-method, representing the distance from the centroid of each layer to the global neutral axis.

The shear stiffness of beam B, $S^B = (GA)_B$, is defined as:

$$S^B = \left( \frac{1}{a^2} \right) \left[ \sum_{i=1}^{n-1} \frac{1}{k_{i,i+1}} + \frac{h_1}{2 \cdot G_1 \cdot b_1} + \sum_{i=2}^{n-1} \frac{h_i}{G_i \cdot b_i} + \frac{h_n}{2 \cdot G_n \cdot b_n} \right] \tag{6}$$

Here, $k_{i,i+1} = \frac{k_s}{s_i}$ is the slip modulus per unit length for the joint between layers $i$ and $i+1$, $G_i$ is the shear modulus, and $a$ is the panel depth.

### 4.3. Indirect estimation from dynamic tests

As shown in the following section, the first three natural frequencies of the tested specimens correspond to the bending modes of a pinned–pinned beam. The natural frequency $f_n$ of such a beam with constant mechanical properties along its span is given by Eq. (7):

$$f_n = \frac{n^2 \pi}{2L^2} \left( \frac{EI_{\text{dyn}}}{\rho A} \right)^{1/2} \tag{7}$$

To linearize this relationship, both sides of Eq. (7) are squared, resulting in Eq. (8):

$$f_n^2 = \left( \frac{n^2 \pi}{2L^2} \right)^2 \left( \frac{EI_{\text{dyn}}}{\rho A} \right) \tag{8}$$

By rearranging Eq. (8), the dynamic bending stiffness $EI_{\text{dyn}}$ can be isolated, as shown in Eq. (9):

$$EI_{\text{dyn}} = \frac{4L^4 \rho A f_n^2}{n^4 \pi^4} \tag{9}$$

To improve accuracy, a least squares approach is adopted using the first three measured frequencies $f_1$, $f_2$, and $f_3$, corresponding to mode

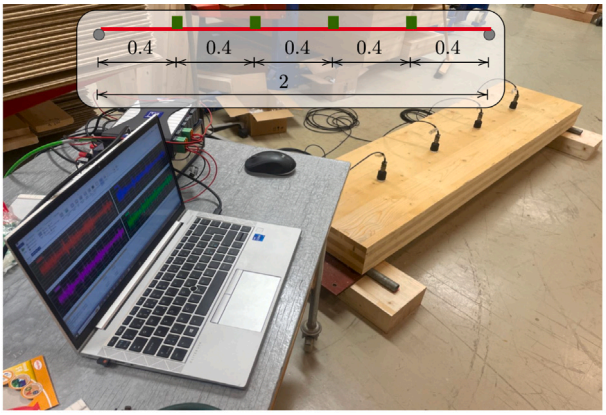


**Fig. 3.** View of the experimental setup for dynamic identification tests. The dimensions are in meters.

numbers $n = 1, 2, 3$. The corresponding system of equations is presented in matrix form in Eq. (10):

$$\begin{bmatrix} f_1^2 \\ f_2^2 \\ f_3^2 \end{bmatrix} = \left( \frac{\pi^4}{4L^4} \right) \frac{EI_{\text{dyn}}}{\rho A} \begin{bmatrix} 1 \\ 4 \\ 9 \end{bmatrix} \tag{10}$$

The least squares estimate of $X = \frac{EI_{\text{dyn}}}{\rho A}$ is calculated according to Eq. (11):

$$X = \frac{\mathbf{C}^T \mathbf{f}^2}{\mathbf{C}^T \mathbf{C}} \tag{11}$$

where $\mathbf{C}$ is the coefficient matrix.

## 5. Description of the experimental tests

The following subsections provide details of the experimental steps conducted and repeated for various levels of MC: (i) dynamic identification, (ii) three-point bending test, (iii) push-out tests and (iv) specimen conditioning in the climate chamber.

### 5.1. Dynamic identification

The authors conducted dynamic identification of the WDCLT panels using the Stochastic Subspace Identification method [49], implemented in the open-source software pyOMA [50,51]. The panel was instrumented with four equidistant accelerometers (PCB 393B12) [52], as shown in Fig. 3. Two tests were performed for each sample: one under ambient excitation and another with a person walking at a natural pace of approximately 2 Hz, weighing 70 kg. Both data acquisitions lasted 20 min and were recorded at a sampling frequency of 200 Hz. The data acquisition system used was CATman by HBK [53]. The tests have been conducted in the Norwegian Institute of Wood Technology laboratory in Oslo, Norway.

The analyses' output is the model parameters regarding natural frequency, mode shapes, and damping ratios.

### 5.2. Three-point bending tests

To evaluate the stiffness of the WDCLT panels, three-point bending tests were conducted (Fig. 4) over a span of 2 m. A steel beam was used to distribute the applied load evenly across the width of the panel. Vertical displacements were recorded using two displacement transducers, which were connected to an HBK data acquisition system. The applied load was monitored using the embedded load cell with a 500 kN capacity.

The tests were carried out at the Norwegian Institute of Wood Technology laboratory in Oslo, Norway. The load was applied at a displacement rate of 1 mm/min until reaching a mid-span deflection equal to $l/300$ following [54]. The stiffness ($EI$) was calculated using Eq. (12).

$$EI = \frac{\Delta P \cdot l_0^3}{\Delta d \cdot 48} \tag{12}$$

Where $\Delta P$ is the load variation, $\Delta d$ is the displacement variation, and $l_0$ is the span. It is worth noting that interlayer slip was not directly measured during the panel bending or dynamic tests. However, based on the load levels applied in these tests, limited to achieving mid-span deflections of $l/300$ in static bending and very low amplitudes in dynamic excitation, it is reasonable to assume that the slip experienced was significantly lower than the displacements observed in the push-out tests at $0.1 \cdot F_{max}$. This supports the use of linear-elastic assumptions in estimating bending stiffness under these conditions.

The panel was supported on wooden bases, as shown in Fig. 4. Although wood is less stiff than steel, the small dimensions of the supports and low load level ensure that their deformation under the applied loads is negligible compared to the panel deflection. Therefore, any contribution of the wooden supports to the measured bending response is considered minimal and does not affect the validity of the results.

### 5.3. Slip modulus estimation

As outlined in Section 4, the bending stiffness prediction requires the connection's slip modulus ($K$). To determine this value, a dedicated push-out test has been carried out by the company BIOHABITAT, see Fig. 5. When the panel is bent, compression and tension forces act in opposite directions, resulting in a slip between the layers since the doweled connection is not perfectly rigid. To simulate the sliding of the top and bottom layers of the WDCLT panel, BIOHABITAT tested a 750 × 180 model consisting of a 6-layer WDCLT panel (layup 180 mm in Fig. 2). The test procedure began with the failure of a pilot specimen to estimate the failure load ($F_{est}$) for the remaining ten specimens. A cyclic loading procedure was followed, starting with the application of a load equal to $0.4 \cdot F_{est}$, holding for 30 s, and then unloading to $0.1 \cdot F_{est}$, holding again for 30 s. The load was then reapplied until either the ultimate load was reached or a 15 mm slip occurred, whichever came first. Displacement measurements were recorded throughout the entire test. The testing machine applied the load at a constant rate, ensuring that either the ultimate force or the 15 mm slip was reached within 5 to 7 min.

The slip modulus of the connection was calculated using the following equation, adapted from EN 26891 [46] and supported by scientific literature [55]:

$$K = \frac{0.4F_{\text{max}} - 0.1F_{\text{max}}}{u_{0.4} - u_{0.1}} \tag{13}$$

This formulation defines the initial slip modulus $K$ as the slope of the force–displacement curve between 10% and 40% of the maximum load per dowel $F_{\text{max}}$. Here, $F_{\text{max}}$, is the experimentally measured maximum force acting on a single dowel, obtained by dividing the total applied force by the total number of dowels in the specimen [kN] equal to 14, $u_{0.1}$ is the average relative displacement between consecutive lamellae at 10% of $F_{\text{max}}$ [mm], $u_{0.4}$ is the average relative displacement between consecutive lamellae at 40% of $F_{\text{max}}$ [mm], and $K$ is the slip modulus of the signle dowel per interface [kN/mm]. The total number of dowels in the specimen is 14, 180 mm long, distributed across three staggered rows containing 5, 4, and 5 dowels, respectively, with a spacing of 150 mm along each row. It is important to note that the displacement measured during the push-out tests corresponds to the total relative slip between the two external lamellae of the six-layer panel. This includes the cumulative slip across five shear interfaces. To obtain a representative slip modulus per single shear plane, consistent with analytical models such as the $\gamma$-method and the SAM, the total measured slip was divided by the number of shear planes (i.e., five). This

**Fig. 4.** Views of the experimental setup of the three-point bending test.

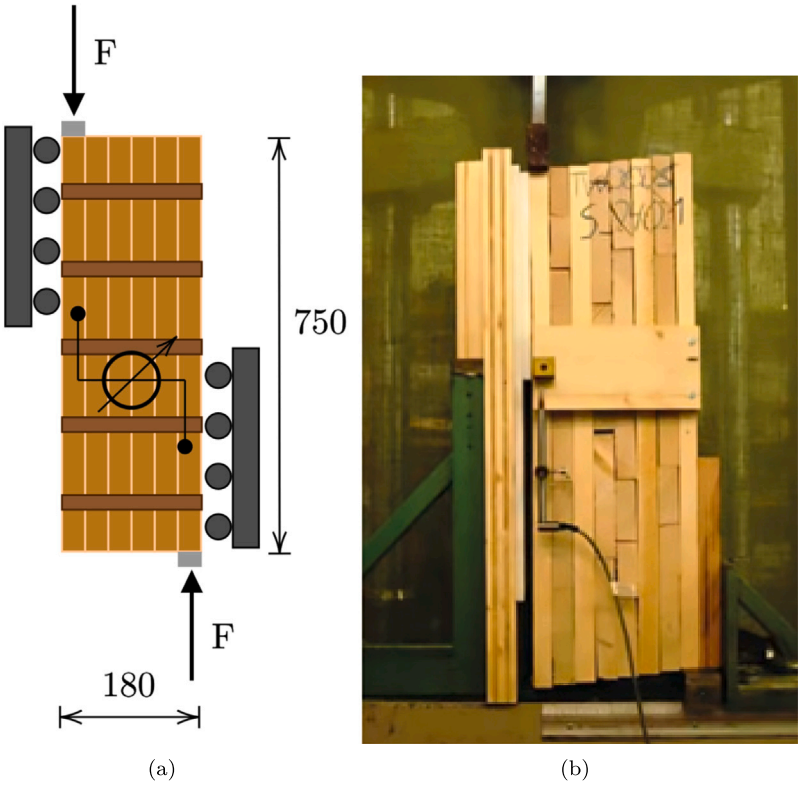


**Fig. 5.** (a) Experimental setup of the push-out tests (b) View of the push-out specimens after the tests.

approach yields an average slip per interface and ensures compatibility with the modeling assumptions. As such, the calculated slip modulus $K$ represents the stiffness of a single dowel acting across one interface. Visual inspection of the test specimens (see Fig. 5(b)) confirms that the slip is distributed uniformly across the lamella interfaces. The displacement increases approximately linearly from the fixed side to the loaded side, indicating that the shear slip between adjacent lamellas is nearly equal. This justifies the assumption of uniform shear deformation and supports the use of average slip (total displacement divided by the number of shear planes) in calculating the slip modulus per interface. It should also be noted that in standard push-out tests, when the connector is loaded in double shear (i.e., between two members symmetrically), a factor of $\frac{1}{2}$ is typically applied to account for slip on both sides.

### 5.4. Hygrothermal conditioning phase

To achieve the target MC values of the WDCLT panels, a controlled conditioning process was conducted in two separate environmental chambers: a drying chamber and a humidification chamber, shown in Fig. 6.

The MC of each panel was measured using a Brookhuis FMD6 handheld moisture meter (also known as the Absolute Moisture Meter FMD 6), manufactured by Brookhuis Applied Technologies B.V. The probe used features 60 mm long electrode pins with an effective penetration depth of approximately 43 mm. Three measurements were taken on each surface of the panel (both faces), and the results were averaged to estimate the representative surface MC. It is noted that this method primarily captures surface moisture and may not fully reflect internal moisture gradients. This is particularly relevant for the 210 mm panels,

(a) (b)

**Fig. 6.** (a) View of the WDCLT panels in the drying room at RH=20% and T=20 °C; (b) View of the humid chamber at RH=80% and T=20 °C.

where higher MC may persist in the inner layers compared to the surface.

The process involved two distinct phases: a drying phase to reduce MC from 12% to 8%, followed by a humidification phase to increase MC to 15%.

It should be remarked that, although MC in internal wall panels can fall below 7% under in-service conditions [45], prolonged conditioning would be required to replicate this in the lab. Due to limited access to the climate chamber, 8% was selected as the lowest MC level achievable within the available timeframe.

During the drying phase, the panels were placed in the chamber at a RH of 20% and a constant temperature of 20 °C. These conditions were maintained to facilitate gradual moisture reduction while minimizing internal stresses and preventing cracks or distortions in the panels. The MC of the panels was monitored using a resistance-based moisture meter every two weeks.

Following the drying phase and the consequent bending tests, the panels were transferred to the humidification chamber to achieve the target MC of 15%. This chamber was maintained at RH = 80% and $T$ = 20 °C to promote moisture absorption. MC was also monitored every two weeks, and the conditioning process continued until the MC stabilized at 15%.

## 6. Experimental results

The experimental results are organized into four subsections, each addressing a specific aspect of the analysis: (i) Estimation of the slip modulus: This part presents the results of the push-out tests, which are used to predict the bending stiffness using the $\gamma$-method or the SAM. (ii) Dynamic identification and three-point bending tests: This subsection analyzes the results from both glued and adhesive-free panels to assess the effects of bonding and excitation levels on the bending stiffness. (iii) Effect of MC on bending stiffness: The EI values are estimated and discussed on for three different MC levels: 12%, 8%, and 15%. (iv) Finally, a discussion part explores how MC influences bending stiffness (EI) and, subsequently, the slip modulus.

### 6.1. Push-out tests for assessing slip modulus

To estimate the bending stiffness using both the $\gamma$-method and the SAM, it is essential to know the mechanical properties of the WDCLT. The mechanical properties are provided in Table 1 and correspond to the C24 strength class.

In particular, the transverse modulus is obtained from the following empirical formula, as reported in [56]:

$$E_{\perp} = \frac{E_{\parallel}}{30} \tag{14}$$

**Table 1**
Average mechanical properties of timber used in assembling the WDCLT panels.

| $\rho$ [kg/m$^3$] | $E_{\parallel}$ [MPa] | $E_{\perp}$ [MPa] | $E_{45}$ [MPa] | $E_{135}$ [MPa] |
|---|---|---|---|---|
| 450 | 11,000 | 367 | 1,900 | 1,900 |

Meanwhile, Hankinson's formula [57] is used to estimate Young's modulus corresponding to a given angle of the fibres relative to the grain direction:

$$E_{\theta} = \frac{E_{\parallel} \cdot E_{\perp}}{E_{\parallel} \cdot \sin^2(\theta) + E_{\perp} \cdot \cos^2(\theta)} \tag{15}$$

where $E_{\parallel}$ is the modulus of elasticity parallel to the grain, $E_{\perp}$ is the modulus of elasticity perpendicular to the grain, and $\theta$ is the angle of the fibres relative to the grain direction. The following analyses were conducted: (i) Prediction of the bending stiffness using the mechanical properties in Table 1 and the slip modulus from the push-out tests. (ii) Optimization of the slip modulus and estimation of a multiplicative factor $\alpha_k$ to minimize the error between the predicted bending stiffness and the one obtained from dynamic tests and three-point bending tests:

$$\hat{K} = \alpha_k K \tag{16}$$

where $\hat{K}$ is the optimal slip modulus and $\alpha_k$ is the optimal multiplier that minimizes the error:

$$\alpha_k = \arg\min_k \left(EI_{\text{exp}} - EI_{\text{model}}\right)^2 \tag{17}$$

where $EI_{\text{exp}}$ is the experimental bending stiffness and $EI_{\text{model}}$ that from the models, either the $\gamma$-method or the SAM.

Table 2 shows the results of the push-out tests, where the force values and slip modulus refer to a single connector per single shear plane.

The connection stiffness, estimated using Eq. (13), is 1.62 kN/mm. This value is consistent with slip modulus values reported in the literature for wooden dowel connections. For example, Pereira et al. [14] report a slip modulus of 1.48 kN/mm for 19 mm Pau-roxo dowels in double-shear configuration, embedded in glued laminated softwood (Pinus taeda and P. elliottii). Although their material and test setup differ from those used in this study, the results are comparable. Their custom test setup was specifically developed to replicate the interlayer slip due to tension–compression and shear during panel bending, diverging from the ISO 6891 standard. In contrast, the current tests involved 16 mm European beech dowels embedded in softwood lamellas under single-shear conditions that reflect actual wall assembly performance.

### 6.2. Dynamic and static bending stiffness estimation

Table 3 presents the results of dynamic identification using the SSI-method [49] implemented through PyOMA [51].

**Table 2**
Results of the push-out tests and slip modulus estimation. $F_{max}$ is the maximum force from push-out tests per single dowel and $u_{0.1}$ and $u_{0.4}$ the average relative displacements between consecutive lamellae corresponding to 0.1 $F_{max}$ and 0.4 $F_{max}$.

| Sample No. | $0.1 \cdot F_{max}$ [kN] | $0.4 \cdot F_{max}$ [kN] | $u_{0.1}$ [mm] | $u_{0.4}$ [mm] | Slip Modulus [kN/mm] |
|---|---|---|---|---|---|
| 1 | 0.98 | 3.93 | 0.3 | 2 | 1.74 |
| 2 | 1.05 | 4.19 | 0.33 | 1.71 | 2.29 |
| 3 | 1.01 | 4.02 | 0.25 | 1.99 | 1.73 |
| 4 | 0.88 | 3.52 | 0.34 | 2.12 | 1.49 |
| 5 | 0.94 | 3.75 | 0.31 | 2.18 | 1.50 |
| 6 | 0.8 | 3.2 | 0.29 | 2.13 | 1.30 |
| 7 | 0.8 | 3.18 | 0.4 | 1.93 | 1.54 |
| 8 | 1.04 | 4.16 | 0.24 | 2.01 | 1.76 |
| 9 | 0.83 | 3.33 | 0.29 | 2.17 | 1.33 |
| 10 | 0.89 | 3.57 | 0.24 | 2.06 | 1.48 |
| Mean | – | – | – | – | 1.62 |
| CoV | – | – | – | – | 0.18 |

**Table 3**
Natural frequencies and damping ratios of the tested specimens and MAC between the mode shapes between forced and operational states.

| Sample | Mode No. | Forced | | Operational | | MAC | Relative Error $f_n$ [%] |
|---|---|---|---|---|---|---|---|
| | | $f_n$ [Hz] | $\xi$ [%] | $f_n$ [Hz] | $\xi$ [%] | | |
| BIO15-1 | 1 | 24.646 | 1.35 | 24.747 | 1.13 | 89 | −0.41 |
| | 2 | 55.930 | 1.28 | 56.827 | 0.80 | 98 | −1.58 |
| | 3 | 89.908 | 1.79 | 91.228 | 1.10 | 94 | −1.45 |
| BIO15-2 | 1 | 26.605 | 1.75 | 26.024 | 1.49 | 95 | 2.24 |
| | 2 | 64.513 | 2.42 | 62.744 | 1.65 | 95 | 2.82 |
| | 3 | 103.816 | 2.13 | 100.344 | 2.48 | 97 | 3.46 |
| BIO15-3 | 1 | 23.388 | 2.04 | 23.865 | 2.16 | 89 | −2.00 |
| | 2 | 51.230 | 1.50 | 51.888 | 1.11 | 91 | −1.27 |
| | 3 | 85.436 | 1.61 | 86.237 | 1.80 | 90 | −0.93 |
| BIO15-4 | 1 | 25.073 | 2.58 | 25.600 | 1.35 | 91 | −2.06 |
| | 2 | 57.764 | 2.29 | 58.742 | 1.57 | 94 | −1.67 |
| | 3 | 101.480 | 2.11 | 100.147 | 3.11 | 95 | 1.33 |
| BIO21-1 | 1 | 33.215 | 1.82 | 32.501 | 1.44 | 92 | 2.19 |
| | 2 | 69.908 | 2.49 | 70.989 | 1.36 | 89 | −1.52 |
| | 3 | 117.851 | 2.60 | 118.021 | 1.81 | 96 | −0.14 |
| BIO21-2 | 1 | 34.521 | 1.34 | 34.892 | 1.35 | 94 | −1.06 |
| | 2 | 70.291 | 2.38 | 69.225 | 2.12 | 94 | 1.54 |
| | 3 | 113.563 | 2.21 | 114.179 | 1.35 | 89 | −0.54 |
| BIO21-3 | 1 | 31.673 | 2.15 | 32.117 | 1.82 | 94 | −1.38 |
| | 2 | 61.591 | 1.71 | 62.720 | 1.21 | 91 | −1.80 |
| | 3 | 109.417 | 1.77 | 110.833 | 1.13 | 96 | −1.28 |
| BIO21-4 | 1 | 32.200 | 1.39 | 32.576 | 0.79 | 89 | −1.15 |
| | 2 | 66.966 | 2.17 | 67.792 | 1.72 | 94 | −1.22 |
| | 3 | 109.409 | 1.98 | 110.593 | 2.01 | 98 | −1.07 |

Two excitation conditions were considered: (i) a low-amplitude operational condition, and (ii) vertical excitation induced by a person performing a sequence of short walking bursts across the 2 m panel at a step frequency of approximately 2 Hz. To investigate potential nonlinear effects in the slip modulus, a 70 kg individual periodically stepped on and off the 2 m panel over a 20 min period, performing short bursts of walking at a step frequency of approximately 2 Hz. This vertical excitation was used to amplify the structural response and assess whether higher excitation levels could mobilize nonlinear interlayer slip, thereby affecting the bending stiffness and the natural frequencies. Notably, the individual was not continuously on the structure. This explains the negligible difference in natural frequencies observed between the two test conditions.

The three modes (see Fig. 7) clearly correspond to the first three flexural modes of a simply supported beam and can therefore be reliably used to estimate the bending stiffness $EI$ using Eq. (11). It is observed that there is no significant difference between the frequencies obtained from the walking tests and those under operational conditions, proving that a walking person does not induce nonlinear effects in the dynamic slip modulus. The relative errors between the measured frequencies are always below 4% in all cases.

Table 4 summarizes the bending stiffness values [Nm$^2$] obtained from three-point static tests, along with those estimated from dynamic tests using Eq. (11). The table also includes the predicted bending stiffness of the WDCLT panels, calculated using both the $\gamma$-method and the SAM. For each case, the percentage difference compared to the static test results is provided. Additionally, Table 5 presents a comparison between the bending stiffness of WDCLT and glued CLT panels with a similar layup. These results are also illustrated in the bar plot in Fig. 8.

The dynamic bending stiffness is significantly higher than that obtained from static bending tests, averaging 2.6 times greater, nearly three times. This difference may seem substantial, particularly for serviceability assessments, as it highlights the inherent flexibility of the panels.

Nevertheless, these panels are not directly comparable in stiffness to their glued counterparts, which are used as benchmarks for assessing the limitations and potential of this structural solution. The bending stiffness of glued CLT with an analogous layup is consistently 13 to 15 times higher, with relative differences exceeding 1000%. This discrepancy could be a limiting factor for the widespread adoption of WDCLT.

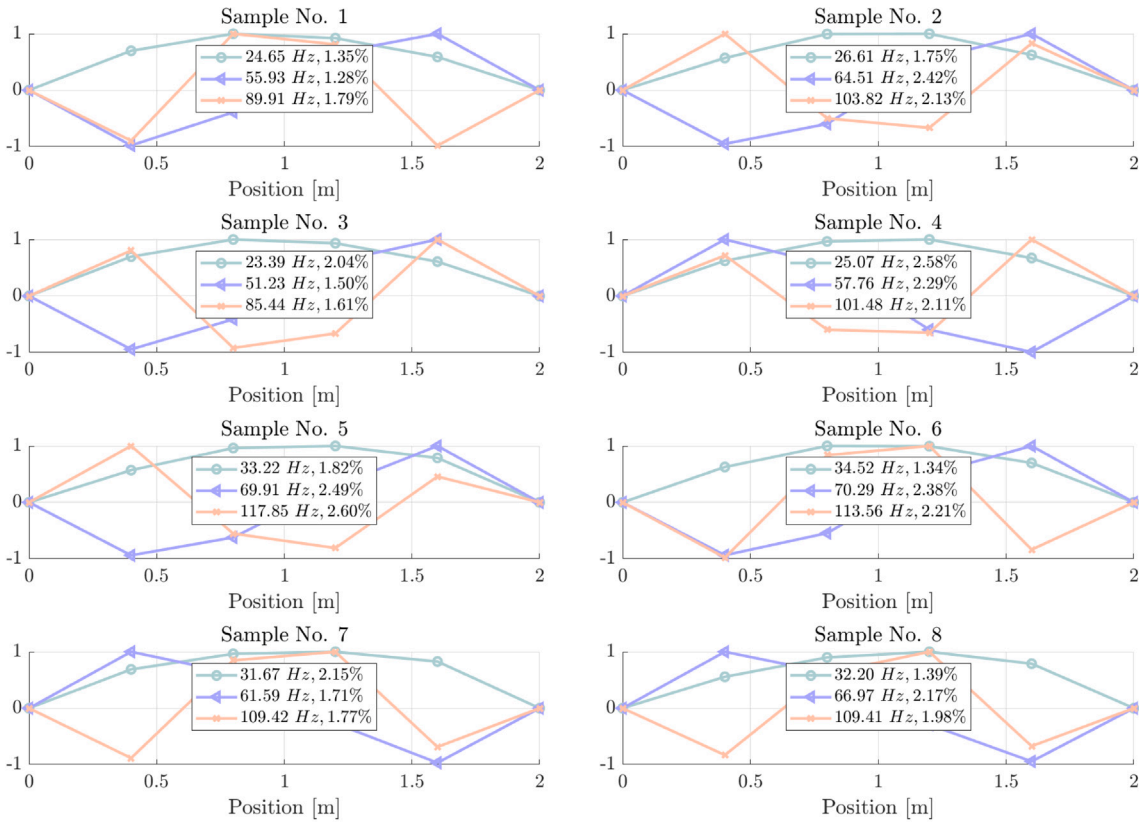


**Fig. 7.** Normalized mode shapes of the tested specimens identified through Operational Modal Analysis (OMA). The $x$-axis indicates sensor position along the panel length, while the $y$-axis represents unitless relative amplitude. All tests were conducted at a moisture content of approximately 12%.

**Table 4**
Synopsis table presenting the bending stiffness [Nm$^2$] estimated from three-point bending tests on WDCLT (Static test), as well as from natural frequencies using Eq. (11) (Dynamic test), along with the corresponding relative difference (Rel. Diff.). The table also shows the predicted bending stiffness of WDCLT obtained using the $\gamma$-method and the SAM. These predictions assume the mechanical properties listed in Table 1 and a slip modulus of 1.62 kN/mm, as determined from push-out tests. All panels had an MC equal to 12%.

| Sample | Experimental Bending Stiffness | | | Gamma-method | | SAM method | |
|---|---|---|---|---|---|---|---|
| | Static [N·m$^2$] | Dynamic [N·m$^2$] | Rel. diff. [%] | Value [N·m$^2$] | Rel. err. [%] | Value [N·m$^2$] | Rel. err. [%] |
| BIO15–1 | 52 124 | 133 069 | 155 | 84 533 | 62 | 55 427 | 6 |
| BIO15–2 | 43 472 | 155 070 | 257 | 84 533 | 94 | 55 427 | 28 |
| BIO15–3 | 52 298 | 119 830 | 129 | 84 533 | 62 | 55 427 | 6 |
| BIO15–4 | 54 760 | 137 720 | 151 | 84 533 | 54 | 55 427 | 1 |
| BIO21–1 | 128 655 | 338 361 | 163 | 164 127 | 28 | 83 234 | −35 |
| BIO21–2 | 126 101 | 365 504 | 190 | 164 127 | 30 | 83 234 | −34 |
| BIO21–3 | 136 529 | 307 671 | 125 | 164 127 | 20 | 83 234 | −39 |
| BIO21–4 | 122 992 | 318 011 | 159 | 164 127 | 33 | 83 234 | −32 |
| Mean | | | 166 | | 48 | | −12 |

**Table 5**
Results of static tests on CLT panels with a layup analogous to WDCLT, their relative difference. All panels had an MC equal to 12%.

| Panel thickness [mm] | No. of plies | Static Test WDCLT [N·m$^2$] | Static Test Glued CLT [N·m$^2$] | Rel. diff. [%] |
|---|---|---|---|---|
| 150 | 5 | 52 124 | 699 531 | 1242 |
| 150 | 5 | 43 472 | 679 869 | 1464 |
| 150 | 5 | 52 298 | 700 199 | 1239 |
| 150 | 5 | 54 760 | 670 301 | 1124 |
| 210 | 7 | 128 655 | 1 846 867 | 1336 |
| 210 | 7 | 126 101 | 1 794 804 | 1323 |
| 210 | 7 | 136 529 | 1 772 498 | 1198 |
| 210 | 7 | 122 992 | 1 801 207 | 1364 |
| | | | | 1286 |

Regarding the accuracy of existing methods in predicting bending stiffness, both the $\gamma$-method, the most commonly used, and the SAM were evaluated. Using a slip modulus estimated from push-out tests, both methods provided reasonable predictions, though with notable differences depending on panel thickness (150 mm vs. 210 mm). The $\gamma$-method tends to overestimate stiffness by approximately 70% and

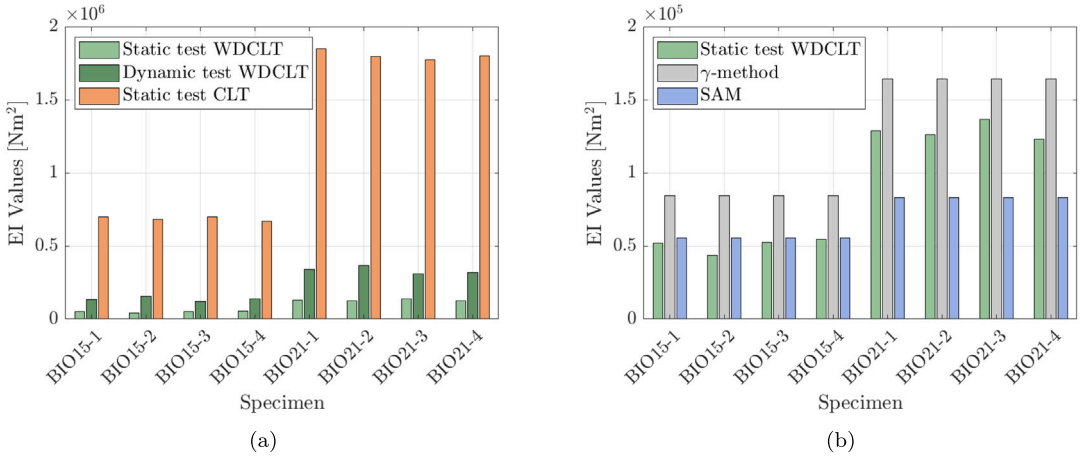


**Fig. 8.** (a) Bar plot of the bending stiffness obtained from static and dynamic tests on WDCLT, along with the bending stiffness of glued CLT with a layup analogous to WDCLT from three-point bending tests. (b) Bar plot comparing the bending stiffness from three-point bending tests on WDCLT with the predictions obtained using the $\gamma$-method and the SAM. The bar plot visually represents the data from Table 4.

**Table 6**
Average and Coefficient of Variation (CoV) of the moisture content in WDCLT panels for the three reference cases.

| Time | Moisture Content | | Time [days] |
|---|---|---|---|
| | Mean [%] | CoV | |
| 28/10/2024 | 11.91 | 5.57 | – |
| 20/12/2024 | 8.10 | 7.50 | 53 |
| 28/02/2025 | 15.20 | 4.55 | 70 |

**Table 7**
Sensitivity of the static bending stiffness to moisture content and relative difference compared to the 12% MC case.

| Sample | MC 12% | MC 8% | | MC 15% | |
|---|---|---|---|---|---|
| | EI [Nm$^2$] | EI [Nm$^2$] | Rel. Diff. [%] | EI [Nm$^2$] | Rel. Diff. [%] |
| BIO15–1 | 52 124 | 33 123 | −36.45 | 58 150 | 75.56 |
| BIO15–2 | 43 472 | 25 871 | −40.49 | 53 157 | 105.47 |
| BIO15–3 | 52 298 | 35 625 | −31.88 | 53 565 | 50.36 |
| BIO15–4 | 54 760 | 29 905 | −45.39 | 55 214 | 84.63 |
| BIO21–1 | 128 655 | 102 905 | −20.01 | 134 654 | 30.85 |
| BIO21–2 | 126 101 | 77 044 | −38.90 | 110 827 | 43.85 |
| BIO21–3 | 136 529 | 98 264 | −28.03 | 129 662 | 31.95 |
| BIO21–4 | 122 992 | 83 758 | −31.90 | 128 016 | 52.84 |
| Mean | | | −34.13 | | 59.44 |

30%, respectively, for the two cases. In contrast, the SAM is more conservative, with significantly lower errors, averaging 12% globally. Specifically, it overestimates bending stiffness by 10% for the 150 mm panel and underestimates it by 35% for the 210 mm panel.

The SAM predicts lower bending stiffness than the $\gamma$-method because it more rigorously accounts for shear deformations, especially in multi-layered timber elements where rolling shear effects in transverse layers play a significant role. Therefore, the SAM gives a more realistic estimate, making it the preferred approach for predicting the bending stiffness of WDCLT panels.

### 6.3. Bending tests before and after climatization

The three-point bending tests were conducted on WDCLT panels under three different MC: 12% (initial condition), approximately 8% after hygrothermal conditioning in a drying chamber, and around 15% after conditioning in a humid chamber. Table 6 presents the average MC and the CoV for the three reference cases. The test dates and the duration required for dry and wet conditioning are also reported, amounting to 53 days for drying and 70 days for humidification.

Table 7 presents the bending stiffness for the three considered MC conditions, as reported in Table 6. Additionally, the relative difference compared to the reference case with an MC of 12% is provided. The same results are graphically represented in Fig. 9 using bar plots.

The effect of MC variation on the bending stiffness of WDCLT is not negligible, unlike in glued CLT panels.

For 150 mm thick panels, the drying process led to a slightly greater reduction in bending stiffness compared to 210 mm thick panels, with decreases of 38% and 30%, respectively. This difference is likely due to the greater thickness of the 210 mm panels, where the core lamellae may have retained higher moisture levels, mitigating the overall reduction in stiffness.

In general, drying had a detrimental effect on the structural integrity of the panels, increasing the risk of slight delamination in the upper layers. As shown in Fig. 10, the drying process caused deformation of the outer lamellae and an increase in the spacing between layers, leading to a reduction in friction and a consequent loss of stiffness.

Regarding the high MC condition (MC = 15%), a complete recovery of bending stiffness was observed, along with an improvement likely associated with the increased friction between layers due to dowel swelling. This recovery was unexpected, as it was initially assumed that the severe environmental conditions and the slight delamination of the outer layer would have irreversibly compromised the panel's integrity. However, this was not the case. Despite the persistent deformation of the outer lamellae caused by drying, their effect on bending stiffness was minimal. Instead, the stiffness recovery was primarily driven by dowel swelling. On average, an increase of 80% and 40% in bending stiffness was observed compared to the 12% MC condition.

Therefore, although the deformations caused by drying are difficult to reverse, they primarily affect non-structural and aesthetic aspects. The swelling of the dowels leads to a full recovery of mechanical performance, restoring the bending stiffness to pre-drying levels.

### 6.4. Discussion

The bending stiffness results obtained so far are difficult to generalize, as a reliable estimation requires the slip modulus, which plays a crucial role in predicting bending capacity and assessing serviceability.

Moreover, in the present case, the effect of MC on the slip modulus, estimated from push-out tests with an average value of 1.62 kN/mm, cannot be neglected. To address this, the authors formulated an optimization problem, as shown in Eq. (16), to determine the slip modulus under both static and dynamic conditions across different MC levels. Table 8 presents the optimal multiplicative factor of the

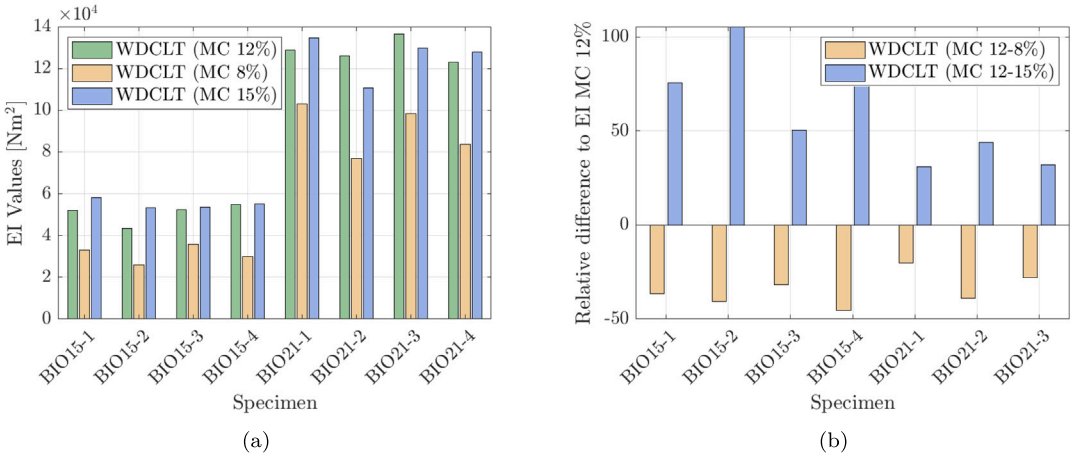


**Fig. 9.** (a) Bar plot of the bending stiffness of each panel corresponding to the three target moisture content values. (b) Variation of the relative difference compared to the reference case at 12% MC.

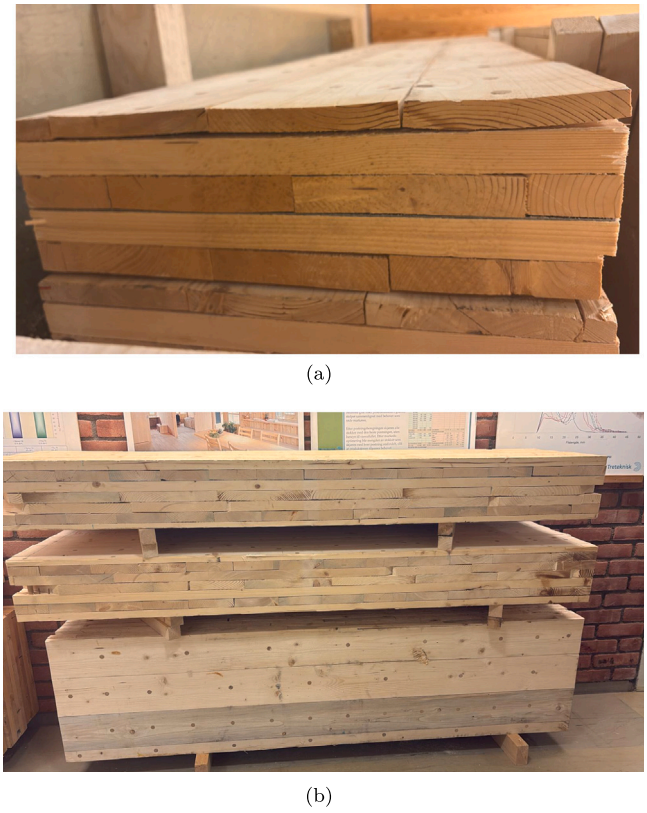


**Fig. 10.** (a) Cross-sections and (b) lateral/front views of the WDCLT at 15% MC showing the gaps between lamellae due to previous drying at MC 8%.

slip modulus required to predict the experimental bending stiffness accurately. Expressing the results in terms of the slip modulus provides a more generalized insight, making the findings applicable to a broader range of cases, unlike bending stiffness, which is highly case-dependent.

The optimization was conducted using the $\gamma$-method, as it is the most commonly employed approach in practical design.

Even under the 12% MC condition, the slip modulus must be reduced to 74% of its initial estimate to achieve accurate predictions. Specifically, for the 5-layer configuration, only 45% of the slip modulus is required, whereas for the 7-layer configuration, the slip modulus estimated from push-out tests is nearly accurate, with a multiplicative factor close to 1.

For 8% MC, the slip modulus multipliers drop further to 0.2 for the 5-layer and 0.4 for the 7-layer configuration, meaning they are slightly less than half of their values at 12% MC. When increasing the MC to 15% MC, the multipliers return to 0.54 and 1, respectively.

Regarding the effect of MC, a high-fidelity mechanical model would be needed to fully understand how moisture influences dimensional expansion, friction between layers, and, consequently, shear interaction. Nonetheless, a general trend can be observed: A 35% average reduction in bending stiffness (from 12% to 8% MC) corresponds to a greater decrease in slip modulus, averaging 60%. Conversely, an increase of nearly 60% in bending stiffness (from 12% to 15% MC) results in only a minor increase in slip modulus by less than 10%.

This discrepancy arises because bending stiffness does not scale linearly with the slip modulus. The more bending stiffness decreases, the more significantly the slip modulus is reduced. However, when bending stiffness increases, the resulting increase in slip modulus is much smaller.

## 7. Conclusions

This experimental study aimed to investigate the sensitivity of in-plane bending stiffness of wooden-doweled CLT (WDCLT) panels, a fully adhesive-free solution, to moisture content (MC) variations, static and dynamic loading conditions, and to compare their performance with conventionally glued CLT panels of similar layups. It has been found that WDCLT panels exhibit a significant reduction in bending stiffness compared to their glued counterparts.

The study considered two layup configurations (5-layer and 7-layer), with four specimens per group, leading to the following key findings: (i) Glued CLT panels demonstrated 12 to 15 times higher bending stiffness compared to WDCLT. (ii) The bending stiffness of WDCLT estimated from dynamic identification tests under walking and operational conditions was approximately 2.6 times higher than that obtained from static three-point bending tests. (iii) Predictions using the $\gamma$-method were found not to be conservative, while the shear analogy method provided accurate estimates with relative errors slightly above 12%. (iv) Moisture content variations significantly influenced bending stiffness: A decrease from 12% to 8% MC led to an average stiffness reduction of 34%. An increase from 12% to 15% MC resulted in a stiffness improvement of 60%.

These findings reveal the critical role of dowel dimensional stability, which is directly influenced by moisture content. Since friction between layers and assembly integrity rely on dowel expansion, a reduction in MC leads to dowel shrinkage, weakening the interlayer interaction and reducing structural performance. However, these stiffness losses

**Table 8**
Optimal multiplier of the slip ($\alpha$) modulus for all tests (static and dynamic, at 12, 8, and 15% MC) to best predict the experimental bending stiffness using the $\gamma$-method. The first column shows the slip modulus, then following are the multipliers corresponding to the slip modulus under dynamic tests, static tests at 12, 8 and 15% MC.

| Sample | MC 12% | MC 12% | | MC 8% | MC 15% |
|---|---|---|---|---|---|
| | $K$ [N/mm] (Push-out tests) | $\alpha$ MC=12% Dynamic | $\alpha$ MC=12% Static | $\alpha$ MC=8% Static | $\alpha$ MC=15% Static |
| BIO15-1 | 1690 | 2.85 | 0.41 | 0.22 | 0.68 |
| BIO15-2 | 1690 | 3.75 | 0.43 | 0.20 | 0.46 |
| BIO15-3 | 1690 | 2.35 | 0.42 | 0.31 | 0.48 |
| BIO15-4 | 1690 | 3.05 | 0.53 | 0.25 | 0.55 |
| BIO21-1 | 1690 | 3.6 | 0.96 | 0.60 | 1.15 |
| BIO21-2 | 1690 | 4.05 | 0.97 | 0.59 | 1.02 |
| BIO21-3 | 1690 | 3.1 | 0.98 | 0.53 | 1.06 |
| BIO21-4 | 1690 | 3.25 | 0.89 | 0.49 | 1.03 |
| | Mean | 3.25 | 0.70 | 0.40 | 0.80 |
| | CoV | 0.17 | 0.39 | 0.43 | 0.36 |

are fully reversible, as evidenced by the substantial stiffness recovery when MC increased from 12% to 15%, despite manifest deformations in the outer lamellae. Additionally, the study demonstrated that the slip modulus does not scale linearly with bending stiffness. The more significant the reduction in stiffness, the more pronounced the decrease in slip modulus, whereas increasing stiffness results in diminishing gains in slip modulus as the structure approaches a condition of maximum interlayer collaboration.

While WDCLT panels offer environmental benefits, they do not provide the same versatility as glued CLT, particularly in applications requiring high bending stiffness. Even a slight reduction in MC below 12% can cause a substantial loss of interlayer collaboration, which is especially problematic for flooring applications, where layer separation may occur. WDCLT should be used for applications where the interaction with outdoor environmental conditions helps maintain an MC level that preserves panel integrity and performance.

## CRediT authorship contribution statement

**Angelo Aloisio:** Writing – review & editing, Writing – original draft, Visualization, Validation, Supervision, Software, Resources, Project administration, Methodology, Investigation, Funding acquisition, Formal analysis, Data curation, Conceptualization. **Dag Pasquale Pasca:** Writing – review & editing, Writing – original draft, Visualization, Validation, Supervision, Software, Resources, Project administration, Methodology, Investigation, Funding acquisition, Formal analysis, Data curation, Conceptualization. **Roberto Tomasi:** Visualization, Validation, Resources. **Massimo Fragiacomo:** Writing – review & editing, Visualization, Supervision.

## Declaration of competing interest

All authors have participated in (a) conception and design, or analysis and interpretation of the data; (b) drafting the article or revising it critically for important intellectual content; and (c) approval of the final version.

This manuscript has not been submitted to, nor is under review at, another journal or other publishing venue.

The authors have no affiliation with any organization with a direct or indirect financial interest in the subject matter discussed in the manuscript.

## Acknowledgments

This work was developed in the framework of the COST Action CA20139 – “Holistic design of taller timber buildings (HELEN)”, and it is the outcome of the Short-Term Scientific Mission (STSM) Grant of the first author – Ref. E-COST-GRANT-CA20139-1d456e25. This study was co-funded by the Norwegian Institute of Wood Technology. The authors thank BIOHABITAT Srl for supplying the tested Wooden Doweled CLT panels.

## Data availability

Data will be made available on request.

## References

[1] R. Brandner, G. Flatscher, A. Ringhofer, G. Schickhofer, A. Thiel, Cross laminated timber (clt): overview and development, Eur. J. Wood Wood Prod. 74 (3) (2016) 331–351, http://dx.doi.org/10.1007/s00107-015-0999-5.
[2] A. Sandoli, C. D’Ambra, C. Ceraldi, B. Calderoni, A. Prota, Sustainable cross-laminated timber structures in a seismic area: Overview and future trends, Appl. Sci. 11 (5) (2021) 1–24, http://dx.doi.org/10.3390/app11052078.
[3] X. Cadorel, R. Crawford, Life cycle analysis of cross laminated timber in buildings: a review.
[4] S. Pei, J.W. van de Lindt, M. Popovski, J.W. Berman, J.D. Dolan, J. Ricles, et al., Cross-laminated timber for seismic regions: Progress and challenges for research and implementation, J. Struct. Eng. 142 (2016) http://dx.doi.org/10.1061/(ASCE)ST.1943-541X.0001192.
[5] M. Izzi, D. Casagrande, S. Bezzi, D. Pasca, M. Follesa, R. Tomasi, Seismic behaviour of cross-laminated timber structures: A state-of-the-art review, Eng. Struct. 170 (2018) 42–52, http://dx.doi.org/10.1016/j.engstruct.2018.05.060.
[6] H. Lim, S. Tripathi, J.D. Tang, Bonding performance of adhesive systems for cross-laminated timber treated with micronized copper azole type c (mca-c), Constr. Build. Mater. 232 (2020) 117208, http://dx.doi.org/10.1016/j.conbuildmat.2019.117208.
[7] S.L. Zelinka, K. Sullivan, S. Pei, N. Ottum, N.J. Bechle, D.R. Rammer, et al., Small scale tests on the performance of adhesives used in cross laminated timber (clt) at elevated temperatures, Int. J. Adhes. Adhes. 95 (2019) http://dx.doi.org/10.1016/j.ijadhadh.2019.102436.
[8] A. Sotayo, D.F. Bradley, M. Bather, M. Oudjene, I. El-Houjeyri, Z. Guan, Development and structural behaviour of adhesive free laminated timber beams and cross laminated panels, Constr. Build. Mater. 259 (2020) 119821, http://dx.doi.org/10.1016/j.conbuildmat.2020.119821.
[9] L. Han, A. Kutnar, J. Sandak, I. Šušteršič, D. Sandberg, Adhesive-and metal-free assembly techniques for prefabricated multi-layer engineered wood products: A review on wooden connectors, Forests 14 (2) (2023) 311, http://dx.doi.org/10.3390/f14020311.
[10] P. Nakos, C. Achelonoudis, E. Papadopoulou, E. Athanassiadou, E. Karagiannidis, Environmentally-friendly adhesives for wood products used in construction applications, in: World Conference on Timber Engineering, WCTE, 2016.
[11] M.H. Hussin, N.H. Abd Latif, T.S. Hamidon, N.I. Idris, R. Hashim, J.N. Appaturi, et al., Latest advancements in high-performance bio-based wood adhesives: A critical review, J. Mater. Res. Technol. 21 (2022) 3909–3946, http://dx.doi.org/10.1016/j.jmrt.2022.10.156.
[12] Eta-23/0041, Lignoloc® Wood-Based Dowel Type Fasteners, Tech. rep, 2023.
[13] Z-9.1-899, Tragende Holzverbindungen Unter Verwendung Von Lignoloc® Holznägeln, Tech. rep, 2020.
[14] M.C.d.M. Pereira, L.A. Pascal Sohier, T. Descamps, C.C. Junior, Doweled cross laminated timber: Experimental and analytical study, Constr. Build. Mater. 273 (2021) 121820, http://dx.doi.org/10.1016/j.conbuildmat.2020.121820.
[15] C. Sandhaas, P. Schädle, Joint properties and earthquake behaviour of buildings made from dowel-laminated timber, in: 16th World Conference on Earthquake Engineering, 16WCEE, 2017.
[16] L. Giordano, M. Derikvand, G. Fink, Bending properties and vibration characteristics of dowel-laminated timber panels made with short salvaged timber elements, Buildings 13 (1) (2023) 99, http://dx.doi.org/10.3390/buildings13010199.
[17] C. O’Ceallaigh, A.M. Harte, P.J. Mcgetrick, Dowel laminated timber elements manufactured using compressed wood dowels, in: Civil Engineering Research in Ireland, CERI 2022, 2022, pp. 222–227.

[18] A. Sotayo, D. Bradley, M. Bather, P. Sareh, M. Oudjene, I. El-Houjeyri, A.M. Harte, S. Mehra, C. O'Ceallaigh, P. Haller, et al., Review of state of the art of dowel laminated timber members and densified wood materials as sustainable engineered wood products for construction and building applications, Dev. the Built Environ. 1 (2020) 100004.
[19] J.-F. Bocquet, A. Pizzi, A. Despres, H.R. Mansouri, L. Resch, D. Michel, et al., Wood joints and laminated wood beams assembled by mechanically-welded wood dowels, J. Adhes. Sci. Technol. 21 (4) (2007) 301–317, http://dx.doi.org/10.1163/156856107780684585.
[20] A.C.C. Viana, F.G. Ebersbach, P.D. de Moraes, W.L. Weingaertner, Influence of pre-drilling hole and feed rate on welded surface strength of pine-itauba joints, Case Stud. Constr. Mater. 17 (2022) e01473.
[21] J.J.E. Biwôlé, A.B. Biwolé, A. Pizzi, J.Z. Mfomo, C. Segovia, A. Ateba, et al., A review of the advances made in improving the durability of welded wood against water in light of the results of african tropical woods welding, J. Renew. Mater. 11 (3) (2023) 1077–1099, http://dx.doi.org/10.32604/jrm.2023.024079.
[22] C. O'Loinsigh, M. Oudjene, H. Ait-Aider, P. Fanning, A. Pizzi, E. Shotton, et al., Experimental study of timber-to-timber composite beam using welded-through wood dowels, Constr. Build. Mater. 36 (2012) 245–250, http://dx.doi.org/10.1016/j.conbuildmat.2012.04.118.
[23] P. Grönquist, T. Schnider, A. Thoma, F. Gramazio, M. Kohler, I. Burgert, et al., Investigations on densified beech wood for application as a swelling dowel in timber joints, Holzforschung 73 (6) (2019) 559–568, http://dx.doi.org/10.1515/hf-2018-0106.
[24] J. Branco, T. Descamps, Analysis and strengthening of carpentry joints, Constr. Build. Mater. 97 (2015) 34–47, http://dx.doi.org/10.1016/j.conbuildmat.2015.05.089.
[25] B.-H. Xu, S.-Y. Jiao, B.-L. Wang, A. Bouchaïr, Mechanical performance of timber-to-timber joints with densified wood dowels, J. Struct. Eng. 148 (4) (2022) 04022023, http://dx.doi.org/10.1061/(ASCE)ST.1943-541X.0003317.
[26] J. Judd, F. Fonseca, C. Walker, P. Thorley, Tensile strength of varied-angle mortise and tenon connections in timber frames, J. Struct. Eng. 138 (5) (2012) 636–644, http://dx.doi.org/10.1061/(ASCE)ST.1943-541X.0000468, cited By 20..
[27] J. Milch, J. Tippner, M. Brabec, V. Sebera, J. Kunecký, M. Kloiber, H. Hasníková, Experimental testing and theoretical prediction of traditional dowel-type connections in tension parallel to grain, Eng. Struct. 152 (2017) 180–187, http://dx.doi.org/10.1016/j.engstruct.2017.08.067, cited By 12.
[28] A. Vilguts, S.Ø. Nesheim, H. Stamatopoulos, K.A. Malo, A study on beam-to-column moment-resisting timber connections under service load, comparing full-scale connection testing and mock-up frame assembly, Eur. J. Wood Wood Prod. 80 (4) (2022) 753–770.
[29] A. Vilguts, H. Stamatopoulos, K.A. Malo, Experimental and analytical evaluation of semi-rigid timber connection with screwed-in threaded rods and steel coupling part, J. Build. Eng. (2024) 109923.
[30] A. Vilguts, A.R. Phillips, R. Jerves, C. Antonopoulos, D. Griechen, Monotonic testing of single shear-plane clt-to-clt joint with hardwood dowels, J. Build. Eng. 88 (2024) 109252.
[31] M. Riggio, J. Sandak, A. Sandak, Densified wooden nails for new timber assemblies and restoration works: A pilot research, Constr. Build. Mater. 102 (2016) 1084–1092, http://dx.doi.org/10.1016/j.conbuildmat.2015.06.045, cited By 33.
[32] G. Ruan, G. Filz, G. Fink, Shear capacity of timber-to-timber connections using wooden nails, Wood Mater. Sci. Eng. 17 (1) (2022) 20–29, http://dx.doi.org/10.1080/17480272.2021.1964595, cited By 14.
[33] C. Ceraldi, V. Mormone, E. Russo Ermolli, Restoring of timber structures: Connections with timber PegsCited by 1, 2008.
[34] C. Ceraldi, M. Lippiello, E. Russo Ermolli, Connections with timber pins: The influence of dowel-bearing StrengthCited by 1, 2011.
[35] C. Ceraldi, M. Lippiello, E. Russo Ermolli, Timber pins connections: Reliability of bolted joints design RulesCited by 1, 2012.
[36] F. Frontini, J. Siem, R. Renmælmo, Load-carrying capacity and stiffness of softwood wooden dowel connections, Int. J. Arch. Herit. 14 (03) (2020) 376–397, http://dx.doi.org/10.1080/15583058.2018.1547798.
[37] Y. Pranata, A. Kristianto, A. Darmawan, Elastic cross-section modulus ratio of jabon (anthocephalus cadamba miq.) bolt-laminated timber beams, IOP Conf. Ser. Mater. Sci. Eng. 1071 (1) (2021) 012016, http://dx.doi.org/10.1088/1757-899X/1071/1/012016.
[38] J.F. Miller, R.J. Schmidt, W.M. Bulleit, New yield model for wood dowel connections, J. Struct. Eng. 136 (10) (2010) 1255–1261, http://dx.doi.org/10.1061/(ASCE)ST.1943-541X.0000224.
[39] K. Jung, A. Kitamori, K. Komatsu, Evaluation on structural performance of compressed wood as shear dowel, Holzforchung 62 (04) (2008) 461–467, http://dx.doi.org/10.1515/HF.2008.073.
[40] X. Bohan, J. Shiyuan, W. Bilin, et al., Mechanical performance of timber-to-timber joints with densified wood dowels, J. Struct. Eng. 148 (04) (2022) 04022023, http://dx.doi.org/10.1061/(ASCE)ST.1943-541X.0003317.
[41] M. Derikvand, S. Hosseinzadeh, G. Fink, Mechanical properties of dowel laminated timber beams with connectors made of salvaged wooden materials, J. Archit. Eng. 27 (4) (2021) 04021035.
[42] BIOHABITAT, Biohabitat - sustainable wooden construction, 2025, URL https://www.biohabitat.it.
[43] International Organization for Standardization, Wood – determination of moisture content for physical and mechanical tests, Geneva, Switzerland, 2020.
[44] ASTM International, Standard test methods for direct moisture content measurement of wood and wood-base materials, 2020, http://dx.doi.org/10.1520/D4442-20.
[45] A. Aloisio, D.P. Pasca, B. Kurent, R. Tomasi, Long-term continuous dynamic monitoring of an eight-story clt building, Mech. Syst. Signal Process. 224 (2025) 112094.
[46] CEN, En 1995 eurocode 5: Design of timber structures, 2004.
[47] H. Kreuzinger, Mechanically Jointed Members and Clt Elements, 2017, pp. 249–262, Ch. 7.
[48] H. Kreuzinger, Flächentragwerke–platten, scheiben und schalen–berechnungsmethoden und beispiele, 1999, pp. 43–60, Informationsdienst Holz, Brücken Aus Holz.
[49] B. Peeters, G. De Roeck, Reference-based stochastic subspace identification for output-only modal analysis, Mech. Syst. Signal Process. 13 (6) (1999) 855–878.
[50] D.P. Pasca, A. Aloisio, M.M. Rosso, S. Sotiropoulos, Pyoma and pyoma_gui: a python module and software for operational modal analysis, SoftwareX 20 (2022) 101216.
[51] D.P. Pasca, D.F. Margoni, M.M. Rosso, A. Aloisio, Pyoma2: An open-source python software for operational modal analysis, in: International Operational Modal Analysis Conference, Springer, 2024, pp. 423–434.
[52] PCB Piezotronics, Model 393b12 seismic ICP accelerometer datasheet, 2025.
[53] HBK (Hottinger Brüel & Kjær), data acquisition systems and instruments, 2025, URL https://www.hbkworld.com/en/solutions/applications/data-acquisition-analysis.
[54] M.C. de Moraes Pereira, L.A.P. Sohier, T. Descamps, C.C. Junior, Doweled cross laminated timber: Experimental and analytical study, Constr. Build. Mater. 273 (2021) 121820.
[55] J. Branco, P. Cruz, M. Piazza, Experimental analysis of laterally loaded nailed timber-to-concrete connections, Constr. Build. Mater. 23 (1) (2009) 400–410.
[56] H.J. Blaß, C. Sandhaas, Timber Engineering-Principles for Design, KIT scientific publishing, 2017.
[57] D.E. Breyer, Design of wood structures, 1988.